Atomistic modelling of thin film argon evaporation over different solid surfaces at different wetting conditions

Mohammad Nasim Hasan ✉, *Sheikh Mohammad Shavik, Khaled Mosharraf Mukut, Kazi Fazle Rabbi, A H M Faisal*

Department of Mechanical Engineering, Bangladesh University of Engineering & Technology (BUET), Dhaka 1000, Bangladesh
✉ *E-mail: nasim@me.buet.ac.bd*

Published in Micro & Nano Letters; Received on 5th May 2017; Revised on 30th October 2017; Accepted on 10th November 2017

In the present study, non-equilibrium molecular dynamics (MD) simulations have been performed to reveal the effect of solid–liquid interfacial wettability on the evaporation characteristics of thin liquid argon film placed over the flat solid surface. The atomistic model considered herein comprises of a three-phase simulation domain having a solid wall over which liquid argon and argon vapour co-exist. Initially, the system is thermally equilibrated at 90 K for a while after which rapid increase in the solid wall temperature induces a phase change process, i.e. evaporation. Both hydrophilic and hydrophobic wetting conditions of the solid surface have been considered at an evaporation temperature of 130 K for three different surface materials such as platinum, silver, and aluminium. The simulation results show that both the surface wettability and surface material have a significant role in phase transition phenomena of thin liquid film, particularly the surface wettability for the present system configuration. The thermal transport phenomena between the wall and liquid thin film have been studied thoroughly and discussed in terms of wall heat flux, evaporative mass flux, upper bound of maximum possible heat flux etc. The results obtained in the present MD simulation study are compared with the macroscopic predictions based on classical thermodynamics. Interestingly, a very good agreement has been found indicating that macroscopic thermodynamics approach can predict the characteristic of phase change phenomena of nanoscale thin liquid film.

Nomenclature

h_{fg}	latent heat of vaporisation [J/kg]
$\dot{m}_{avg}$	time averaged mass flux [kg/m^{2}s]
P	pressure [bar]
q_w	wall heat flux [W/m^2]
q_{avg}	time averaged heat flux observed in the current study [W/m^2]
q_{Therm}	time averaged heat flux as predicted by classical thermodynamics [W/m^2]
$q_{max,max}$	theoretical maximum value of heat flux [W/m^2]
R	ideal gas constant [J/kg-K]
r	inter-molecular distance [Å]
t	time [ns]
t^*	instance at which the non-evaporating layer form in hydrophilic cases [ns]
T	temperature [K]
T_{avg}	time averaged temperature [K]
T_w	wall temperature [K]
x	coordinate along X-axis
y	coordinate along Y-axis
z	coordinate along Z-axis
ε	energy parameter [eV]
σ	length parameter [Å]
φ	energy [eV]
ρ_v	vapour density [kg/m^3]

1. Introduction: Phase change characteristics of thin film liquid have gained substantial attention as it appears in many contexts of engineering applications such as turbine blade tip cooling, thin film evaporators, cooling of the nuclear fuel rod, laser mirror, polymer electrolyte membrane fuel cell and so on. Current advancement in performance, as well as miniaturisation of high power-density electronic circuits (e.g. high-speed microprocessor and insulated gate bipolar transistor circuits), demand high capacity sophisticated thermal management system to avoid possible 'Hot Spot' problem. The role of thin film evaporation is this context is very crucial as it has much potential for energy transport in comparison to traditional nucleate boiling. The efficacy of thin film evaporation for energy transport mainly arises from reduced thermal resistance due to its small thickness. Therefore, investigation of the phase transition characteristics of thin liquid films has become a very popular topic among researchers in recent time. Both experimental and numerical studies have been made on thin film liquid phase change process over the last two decades but there is still deficient in a well-established theory to describe the evaporation behaviours. As space and time scale of the thin film phase change process is very small, conducting experimentation is very difficult. Therefore, many researchers have adopted a numerical approach to study thin film liquid phase change characteristics, particularly using molecular dynamics (MD) simulations. MD simulation has the ability to deal the system in atomic scale and due to this; it is now getting more and more prevalent in the study of thin film phase change phenomena as well as related thermo-physical properties of materials in nanoscale.

A major focus of contemporary MD studies covers various aspects of the phase change behaviour. Kimura and Maruyama [1] numerically studied heterogeneous nucleation of liquid argon (Ar) droplets over isothermal heat baths using phantom molecules. Yu and Wang [2] observed the effect of rapid heating on a thin film of liquid Ar in a nanoconfinement to explain the boiling characteristics and calculated the time averaged mass flux. They confirmed the presence of a 'non-evaporating layer' formed during evaporation and compared it with theoretical models. MD simulations were carried out by Nagayama *et al.* [3] to examine the behaviour of bubbles in a nanoconfined channel and observe the associated nucleation phenomenon. Maroo and Chung [4] performed MD simulations over platinum (Pt) heater and observed the nanoscale liquid film boiling of Ar along with the colloidal adsorption characteristics. Cylindrical nanoposts had been considered in the MD simulations performed by Morshed *et al.* [5] to study explosive

boiling and evaporation of thin liquid films. Apart from atomistic modelling of phase change phenomena, some macroscopic models of explosive boiling have also been reported by Hasan *et al.* [6]. A new dimension can be added to the current researches by considering different nanostructure geometries along with the variation of liquid–solid wettability for different surface materials. The wettability of a solid surface can have major effects on the phase transition characteristics. In the simulations performed by Maruyama and Kimura [7], the contact angle of the bubbles formed during heterogeneous nucleation of Ar over a Pt surface was measured. To understand the effect of surface texture on the liquid film of Ar, Hens *et al.* [8] conducted MD study of liquid Ar over a hot Pt surface and observed that the wetting conditions of the solid surfaces significantly influence the phase change characteristics and bubble nucleation mechanism. Seyf and Zhang [9] have conducted MD simulations to investigate the effect of the size of nanocone array and different types of material such as silver (Ag) and aluminium (Al) on the explosive boiling of an ultra-thin film of Ar at 270 K. Wang *et al.* [10] investigated both explosive boiling (at 310 K) and evaporation (at 150 K) characteristics of a thin film of Ar on an Al flat surface and nanostructured surface. They revealed that the inclusion of nanostructures greatly enhances the heat transfer efficiency and the evaporation rate increases with the height of nanostructure up to a certain height. Most recently, Zhang *et al.* [11, 12] performed MD study to reveal out the influence of solid–liquid interfacial wettability on the phase change transition rate of ultra-thin liquid argon film placed over the Al surface under different wall superheat conditions. They concluded that the heat transfer rate with good wettability (lyophilic) is much higher than bad wettability (lyophobic) for a fixed temperature jump of the system from equilibrium.

This Letter aimed at finding out the effect of solid–liquid interfacial wettability as well as surface material during thin film Ar evaporation. System temperature, spatial number density, heat transfer rate and so on are closely monitored for three different surface materials such as Pt, Ag and Al. The entire system is first equilibrated at 90 K after which it is subjected to an evaporation temperature of 130 K. Selection of different surface materials and evaporation temperature is made according to the contemporary literature. Both hydrophilic and hydrophobic wetting conditions have been taken into consideration. Since atomistic modelling is done during the present simulation according to the lattice structure and no additional roughness is introduced, the surface can be considered as a smooth flat surface. The results obtained from MD study are also compared with the classical thermodynamic predictions.

2. Atomistic model and simulation methodology: The three-phase simulation domain considered in this Letter consists of a solid wall at the bottom end, a thin atomic layer of liquid Ar on top of the solid wall and vapour Ar atoms above the liquid Ar layer. The initial configuration of the simulation domain is shown in Fig. 1, where the dimensions are of 7.35 nm × 70.0 nm × 7.35 nm ($x \times y \times z$). At the bottom of the simulation cuboid it is the solid wall that comprises of eight monolayers solid atoms (Pt/Ag/Al) which are oriented in an FCC (1 0 0) lattice according to their density at 90 K (Pt: 21,500 kg/m^3, Ag: 10,500 kg/m^3 and Al: 2700 kg/m^3). The solid wall has a height of 1.5 nm. Different atomic layers of the solid wall had distinct functions; the bottom most layer is kept fixed during the total duration of the simulation process while the adjacent two layers are taken as the heat source (heater). The remaining layers of atoms on top of the heater are appointed as the solid wall which provides the pathway for heat conduction from the heater to the liquid Ar. The liquid Ar is 3.01 nm thick and arranged according to the density of Ar at 90 K, i.e. 1.367×10^3 kg/m^3. As each metal has a different density as well as the different lattice constant, the system assumes a different number of solid wall atoms for different cases. For example solid wall atom number corresponds to 5476, 5184 and 5004 for Pt, Ag and Al cases, respectively, while the total Ar atom number (liquid and vapour) remains fixed at 4193 in all cases. To avoid possible atomic interference due to the variation of lattice constants for different solid wall materials under consideration, a clearance of 0.1 nm between solid wall and simulation domain has been adopted in the x and z directions.

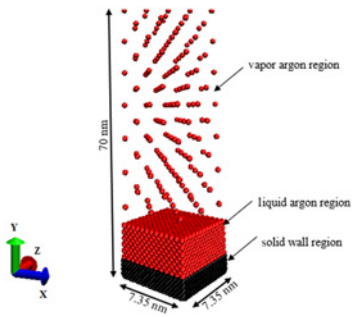

Fig. 1 *Initial configuration of the simulation domain (not true scale)*

The governing equation which calculates the intermolecular forces between the molecules in the present simulation domain is shown in (1), famously known as the Lennard–Jones (LJ) potential [13] equation where σ is the length parameter and ε is the energy parameter. The values of ε and σ for the liquid–liquid (Ar–Ar), solid–solid (Pt–Pt, Ag–Ag and, Al–Al) interactions are tabulated in Table 1. To reduce the simulation time, a cut-off distance is needed to be set. In this Letter, initially, four different cut-off distances are considered, i.e. $3\sigma_{\text{Ar–Ar}}$, $3.5\sigma_{\text{Ar–Ar}}$, $4\sigma_{\text{Ar–Ar}}$ and $4.5\sigma_{\text{Ar–Ar}}$. Since no significant difference in the result is observed between the cut-off distances $4\sigma_{\text{Ar–Ar}}$ and $4.5\sigma_{\text{Ar–Ar}}$, a cut-off distance of $4\sigma_{\text{Ar–Ar}}$ was used for the potential functions for minimising the computational time

$$\begin{aligned} \varphi(r) &= 4\varepsilon\left[\left(\frac{\sigma}{r}\right)^{12} - \left(\frac{\sigma}{r}\right)^{6}\right] \quad \text{for,} \quad r \le \sigma_{\text{cut-off}} \\ \varphi(r) &= 0 \qquad\qquad\qquad\qquad\quad \text{for,} \quad r > \sigma_{\text{cut-off}} \end{aligned} \tag{1}$$

The system configuration of this Letter belongs to a planer case. Hence the periodic boundary condition is applied in the x and z directions, whereas the fixed boundary condition is assumed in the y direction with the adiabatic and elastic wall at the top. That is argon atoms are reflected back into the simulation domain without loss of any energy. These set of boundary conditions are adopted as the entire system is integrated into microcanonical ensemble (NVE) where the number of atoms (N), volume (V) and system energy (E) must be conserved. All the simulations of this numerical study have been performed using the large-scale atomic/molecular massively parallel simulator [14], an open source code, developed by Sandia National Laboratory, USA. The whole simulation process can be described by three distinct steps. In the initial stage, the entire system is subjected to a constant temperature of 90 K using the Langevin–Thermostat and kept in this way for 1 ns. The second stage starts with switching off the Langevin–Thermostat and letting the system to equilibrate by itself for another 1 ns. Various system characteristics such as

Table 1 Potential parameters between different molecules in the simulation domain

Interaction	σ, nm	ε, eV
Ar–Ar	0.3400	0.0104
Pt–Pt	0.2475	0.5200
Ag–Ag	0.2574	0.3510
Al–Al	0.2551	0.4080

doi: 10.1049/mnl.2017.0198

Table 2 Solid–liquid interaction potentials to achieve different surface wettability conditions

Energy parameter	Hydrophilic $\varepsilon_{\text{liquid-solid}}/\varepsilon_{\text{liquid-liquid}} = 2.0$	Hydrophobic $\varepsilon_{\text{liquid-solid}}/\varepsilon_{\text{liquid-liquid}} = 0.5$
$\varepsilon_{\text{liquid-solid}}$	0.0208	0.052

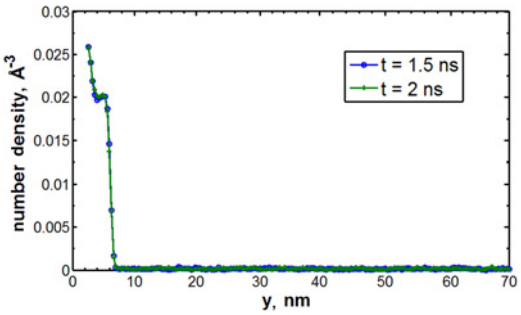

Fig. 2 *Spatial variation of number density of Ar over hydrophilic Pt surface during equilibration*

pressure, temperature, density, and energy are closely monitored to ensure equilibration. At the final stage, the Langevin–Thermostat is turned on again at a higher temperature of 130 K to initiate evaporation and the simulation is run for another 5 ns. Therefore, in total 7 ns of simulation is performed where the first 2 ns is equilibrium MD (EMD) and the rest is non-EMD (NEMD) simulation. A velocity-varlet algorithm with a timestep of 5 fs is used to calculate the velocity of each individual atoms of the system integrated with the microcanonical ensemble (NVE). Visual MD [15] has been used for the visualisation purpose in this Letter.

The effect of surface wettability and materials during the phase transition of argon (Ar) are the major focus of the present study. The different wettability of different surface materials is achieved by assuming different solid-liquid liquid energy potentials ($\varepsilon_{\text{liquid-solid}}$) based on the previous study conducted by Hens *et al.* [8]. Table 2 describes the wettability conditions applied in the present study.

3. Results and discussions: NEMD simulations have been conducted to investigate the phase transition characteristics of thin film liquid Ar over different solid surfaces under different wetting conditions. Since three different materials (Pt, Ag and Al) and two different surface wettability conditions are investigated, a total of six simulations have been conducted during this Letter.

Before performing the NEMD simulations, it is necessary to perform EMD simulations to properly equilibrate the system domain. The EMD simulations were run for first 2 ns. During the equilibrium period, the spatial temperature distribution of Ar and solid wall fluctuated around 90 K for all the cases. To understand the system characteristics during equilibrium the spatial number density profile for two different time instances (1.5 and 2. ns) for hydrophilic Pt surface is shown in Fig. 2 as a representative case. From the comparison of the current number density data with the phase diagrams in the Lenard–Jones system [13] and other studies, it can be assured that the system is in thermal equilibrium. For Ag and Al surfaces and for hydrophobic cases, the number density profiles of Ar during an equilibrium period demonstrate similar characteristics as shown in Fig. 2. Following the initial equilibrium period, each NEMD simulation was run for next 5 ns. In the non-equilibrium part of this MD study, the solid wall temperature (T_w) is increased from 90 to 130 K to induce the desired thin film evaporation process.

The simulation domain snapshots of the hydrophilic and hydrophobic wetting conditions with three different surface materials (Pt/Ag/Al) are shown in Fig. 3. At the initial stages, there is no significant movement of Ar atoms from liquid to vapour region but as the time progresses, the liquid Ar atoms start to escape gradually into the vapour region as individual atoms. In case of hydrophilic surfaces as depicted in Figs. 3*a–c*, this phenomenon occurs more rapidly than the hydrophobic surface as shown in Figs. 3*d–f* as indicated by the contrast of atomic distribution inside the system domain. For hydrophobic surfaces, the system domain appears to be much brighter in comparison to its hydrophilic counterparts. From Fig. 3 for instance, it can be observed that after 7 ns, the thickness of Ar atomic layers adjacent to the hydrophobic solid surface is much larger than in the hydrophilic surfaces for all three different surface materials (Pt/Ag/Al) under consideration. This clearly suggests that hydrophilic surfaces presented more favourable condition for evaporation. This result is in qualitative agreement with the

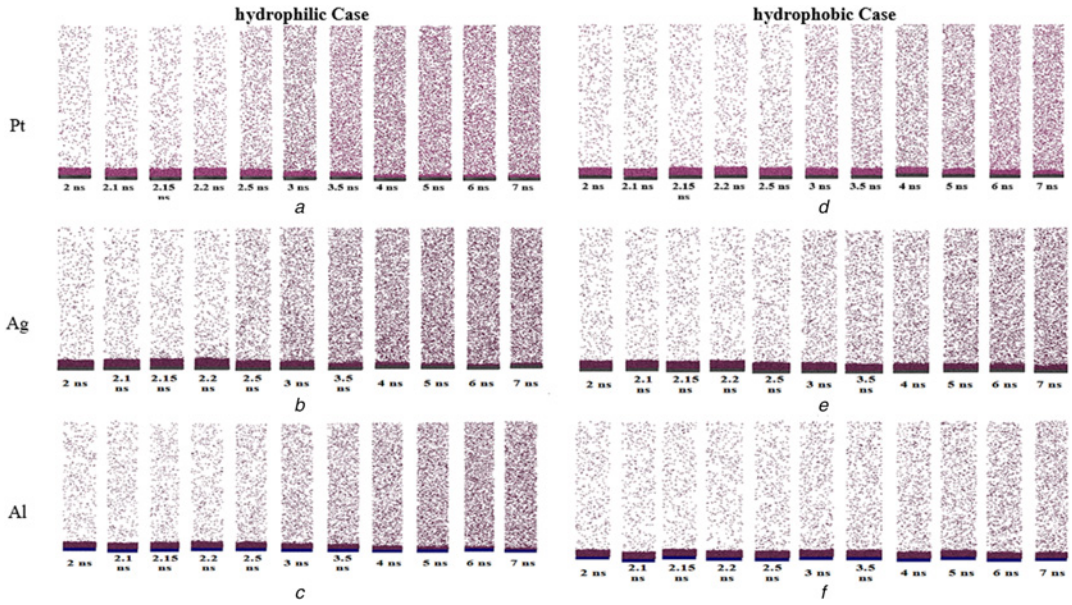

Fig. 3 *Simulation domain snapshots for hydrophilic (left column) and hydrophobic (right column) cases for different surface material*
a–c Hydrophilic case
d–f Hydrophobic case

observation of Zhang *et al.* [11, 12] that a good wetting surface offers faster phase change phenomenon. Apart from hydrophilic/hydrophobic surface wetting condition let us focus on the effect of the surface material on the phase change characteristics. For hydrophilic and hydrophobic cases in Fig. 3 for a particular time instant ($t = 3.5$ and 6 ns, respectively), it is evident that the atomic distribution is denser in cases of Pt and Ag surfaces compared to the Al surface. These observations indicate that Al surface provides the least favourable condition for evaporation among the three different materials under consideration. Also, the amount of Ar atoms in the vicinity of Al surface at the end of simulation time (7 ns) is more than that of Pt and Ag surfaces. This also indicates that the rate of evaporation from the Al surface is the least among the three materials considered in this Letter. This is further discussed in the later sections.

The Ar temperatures for different cases under consideration are shown in Fig. 4. It can be readily observed that the temperature of Ar reaches equilibrium with the solid wall temperature (130 K) much quicker in hydrophilic cases than hydrophobic cases for all the different surface materials (Pt/Ag/Al). This is because of the abundance of liquid Ar atoms near the hydrophilic solid wall which creates a continuous pathway for heat conduction. The rapid increase of temperature in hydrophilic surfaces are indications that the energy is transferred from the solid surface into the liquid Ar layer faster due to the higher solid–liquid interactions. From Fig. 4, it is also seen that, in the cases of hydrophilic surfaces, the Ar temperature reaches equilibrium at 3 ns for Pt surface, at 3.5 ns for Ag surface and at 4 ns for Al surface, respectively. On the other hand, for hydrophobic surfaces, the equilibration of Ar temperature takes more time, i.e. 6 ns for Pt and Ag surfaces. In hydrophobic Al surface, the Ar temperature does not reach the equilibration state within the simulation time. This indicates that the evaporation, as well as heat transfer, is the fastest for Pt surface and least for Al surface among three different surface materials (Pt/Ag/Al) under consideration. These phenomena clearly reveal the fact that energy transfer occurs much easily under hydrophilic wetting condition than the hydrophobic condition.

The temporal pressure distribution in the system for the different cases under consideration is depicted in Fig. 5. Since the volume of the system is constant, the pressure increases with the increase of the temperature and follows a similar trend of temperature as shown in Fig. 4 for all the cases. Higher system pressure for hydrophilic cases compared to hydrophobic cases also indicates more Ar atom remains in the vapour state due to faster evaporation and enhanced energy transfer as indicated in Fig. 3 in terms of dense atomic distribution in the system domain.

To demonstrate the gradual development of phase change process in the simulation domain, let us consider the case of Pt surface as a representative one. Figs. 6 and 7 illustrate the time variation of the number density profiles for Ar over Pt surfaces for hydrophilic and hydrophobic wetting conditions, respectively. As expected, for both cases, as the Ar atoms move away from the liquid layer towards the vapour region with time, the number density of Ar atoms nearby to the solid wall (liquid layers) gradually decreases. From the simulation domain snapshots for Pt surface, as shown in Fig. 3, it is evident that, for hydrophilic cases, the quantity of Ar atoms leaving the liquid layer is much greater than the hydrophobic cases. This fact is confirmed by the number density profile of Ar, as shown in Figs. 6 and 7. For a hydrophilic case as shown in Fig. 6, the spatial number density profiles at 4, 5 and 7 ns overlap one another which indicate the attainment of steady-state configuration. On the other hand, for a hydrophobic case as shown in Fig. 7, the spatial number of density profiles do not overlap each other rather they continue to change pattern indicating that the evaporation is still going on to some degree. From these figures, it is also clear that, as time progresses, the spatial number density of Ar atoms in the vicinity of the wall for hydrophobic cases attains higher values than its hydrophilic counterpart.

It is noteworthy that, Yu and Wang [2] and other researchers reported the existence of a 'non-evaporating layer' adjacent to the solid surface at the end of phase change process. Snapshots of simulation domain in Fig. 3 and spatial number density profiles in Fig. 6 reveal the fact that, for hydrophilic surface after 5 ns, the number of atoms leaving liquid Ar layers are very few or evaporation reaches towards equilibrium and the rest of the Ar atoms in liquid layers remains adjacent to the solid Pt surface as 'non-evaporating layers'. The magnified view of the non-evaporating layer that prevails near the solid hydrophilic surface is depicted in Fig. 8. For hydrophilic surfaces, the non-evaporating layer is almost same for all three materials (Pt/Ag/Al). It indicates that for the current system configuration, the height of the non-evaporative layer only depends on the surface wetting condition and independent of the surface material used. On the other hand, for the hydrophobic case, the number density profile continues to change with time as shown in Fig. 7, indicating the fact that, the evaporation continues to take place in longer time scale in contrast to the hydrophilic case. The magnified view of the liquid layer near the solid surface for a hydrophobic case for all three materials have also been depicted in Fig. 8 from which it is evident that the system belongs to thin film evaporation rather having the state of

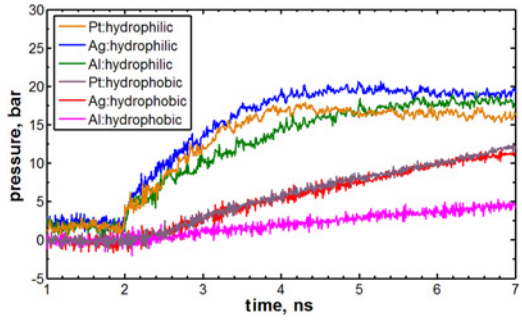

Fig. 5 *Temporal pressure variation in the simulation domain*

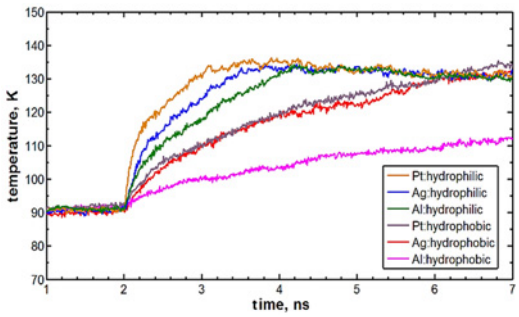

Fig. 4 *Ar temperature variation with time*

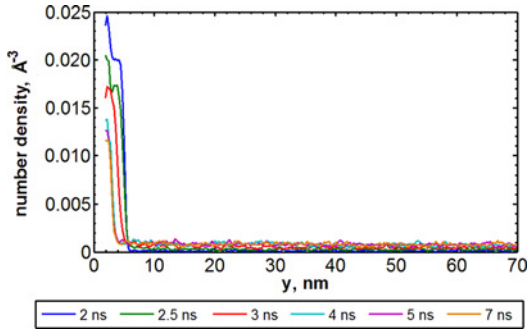

Fig. 6 *Spatial number density variation for hydrophilic Pt surface*

doi: 10.1049/mnl.2017.0198

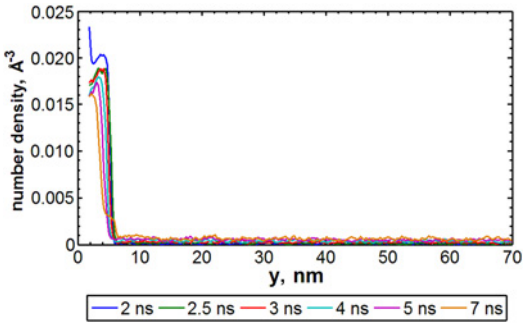

Fig. 7 *Spatial number density variation for hydrophobic Pt surface*

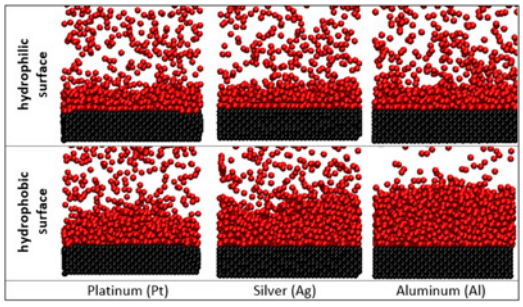

Fig. 8 *Magnified view of the atomistic distribution near the solid walls at 7 ns for different wetting conditions*

'non-evaporating layers' for hydrophobic wall cases. As depicted in Fig. 3, Al surface has the highest number density of Ar atoms adjacent to a solid wall, so among the three materials, Al surface provides a least favourable condition for evaporation. This fact is confirmed by the snap shots as depicted in Fig. 8.

While foregoing discussion focuses on the qualitative assessment of the system characteristics for different surface materials and surface wetting conditions, a better understanding of the system performance is possible if it could be quantified in terms of some transport parameters such as wall heat flux, evaporative mass flux and so on. Heat flux is a crucial tool for quantifying the effectiveness of any heat transfer process. This Letter shows that the energy level of liquid suddenly jumps when the Langevin–Thermostat is switched to 130 K from 90 K, therefore, maximum heat flux occurs just after 2 ns time. Heat flux then decreases with time as shown in Fig. 9. Gambill and Lienhard [16] calculated the theoretical maximum value of heat flux ($q_{max,max}$) using (2), where ρ_v is the vapour density; h_{fg} is the latent heat of vaporisation. The values of the maximum heat flux (q_{max}) observed in this Letter are almost same as the theoretically indicated values calculated using (2). This validates the present atomistic model study. The theoretical maximum values of heat flux ($q_{max,max}$) are compared with the maximum heat flux (q_{max}) obtained in this Letter and tabulated in Table 3

$$q_{max,max} = \rho_v h_{fg} \sqrt{RT/2\pi} \tag{2}$$

An important observation from the heat flux profiles as depicted in Fig. 9 is that the heat flux after reaching the maxima continues to decrease over a much larger time span for hydrophobic cases than hydrophilic cases. This suggests that the rate of evaporation for the hydrophobic surface is much less and this supports the earlier discussion regarding the trajectories of atoms as indicated in Fig. 3 and spatial number density profiles as shown in Figs. 6 and 7.

Fig. 10 delineates the temporal variation of the net evaporation number for different surface materials as well as different surface wetting conditions. It represents the number of atoms that escaped from the liquid zone to the vapour zone. Since the simulation is run to equilibrate for the first 2 ns, the net evaporation number is

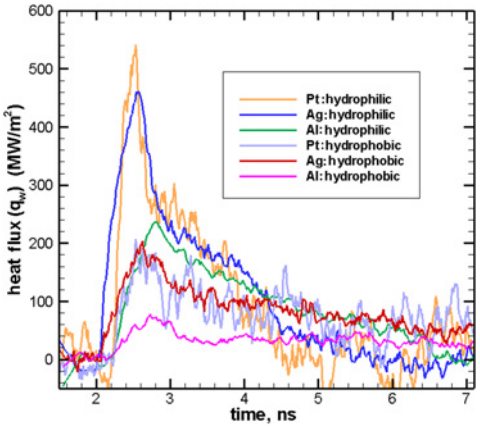

Fig. 9 *Heat flux variation normal to the solid wall*

same for all the cases under consideration. From Fig. 10, it is evident that the evaporation in hydrophilic cases occurs at a much higher rate compared to the hydrophobic cases. It is also obvious that, in hydrophilic cases, the net evaporation number reaches an equilibrium value for all three surface materials (Pt/Ag/Al) while for hydrophobic case continues to rise with time. This variation in the trend firmly agrees with the formation of 'non-evaporating layer' in hydrophilic surfaces as indicated in Fig. 8.

The net evaporation number of hydrophilic surfaces depicted in Fig. 10 indicates that evaporation reaches the equilibrium state at 3.8 ns for Pt surface, 4 ns for Ag surface and 6 ns for Al surface. In case of hydrophobic surfaces, none of these three materials under consideration (Pt/Ag/Al) reaches equilibrium within the simulation time period. However, both the hydrophobic Pt and Ag surfaces demonstrate the similar rate of evaporation while the hydrophobic Al surface has a much lower rate of evaporation. This point indicates the fact that, Pt surface provides the most favourable condition for phase transition while the Al surface provides the least favourable condition under the hydrophobic wetting condition as defined in this Letter.

The time averaged heat flux (q_{avg}) can be calculated by numerical integration of the wall heat flux curve over the timespan of evaporation. Since the present simulations are equilibrated for 2 ns at first, the lower limit of integration has been set as $t_0 = 2$ ns which indicates the onset of heating during simulation. From earlier discussion, it has been observed that non-evaporating layer is formed in all hydrophilic surfaces after the onset of heating of the solid wall at 130 K as indicated by the net evaporation number curve in Fig. 10. Therefore, the time averaged heat flux (q_{avg}) for the hydrophilic surface is calculated until the formation of the non-evaporating layer (i.e. from $t_0 = 2$ ns to $t_f = t^*$). However, on the other hand, in case of hydrophobic surfaces, no such non-evaporating layer forms during the simulation time period. Therefore, for hydrophobic surfaces, the time averaged heat flux (q_{avg}) is calculated by considering the entire time duration of the simulation (i.e. from $t_0 = 2$ ns to $t_f = 7$ ns). In other words, the time averaged heat flux (q_{avg}) is calculated as

$$q_{avg} = \frac{1}{t_f - t_0} \int_{t_0}^{t_f} q_w(t)\, dt \tag{3}$$

where $t_0 = 2$ ns and, $t_f = t^*$ (for hydrophilic cases); and $t_f = 7$ ns (for hydrophobic cases).

The order of the time averaged values of the heat flux as depicted in Table 3 gives us a comparative view of the evaporation characteristics for different materials and surface wettability conditions and helps us better understand the phase change behaviour. From the temporal variation of the net evaporation number, it is possible to

Table 3 Comparison of the predictability of evaporation characteristics between MD and classical thermodynamics

Surface material	Surface wetting conditions									
	Hydrophilic					Hydrophobic				
	$\dot{m}_{avg}$, kg/m^{2}s	q_{Therm}, MW/m^2	q_{avg}, MW/m^2	q_{max}, MW/m^2	$q_{max,max}$ [16], MW/m^2	$\dot{m}_{avg}$, kg/m^{2}s	q_{Therm}, MW/m^2	q_{avg}, MW/m^2	q_{max}, MW/m^2	$q_{max,max}$ [16], MW/m^2
Pt	1622	193	228	560	605	515	64	83	200	206
Ag	1320	163	180	480	481	487	62	82	200	206
Al	1013	133	154	250	250	187	27	36	100	99

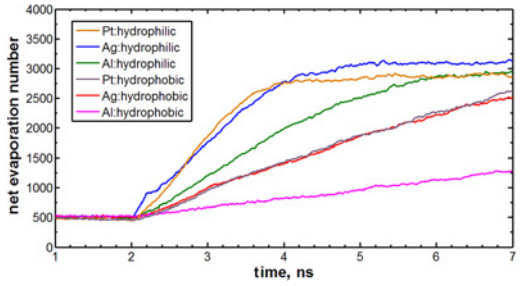

Fig. 10 *Temporal variation of net evaporation number*

calculate the time averaged evaporative mass flux ($\dot{m}_{avg}$) which can be a good indicative of the evaporation characteristics as reported by Nagayama *et al.* [17] and Yu and Wang [2]. Interestingly, by considering the time averaged evaporative mass flux ($\dot{m}_{avg}$) until the non-evaporating layer appears (t^*), one can compare the predictability of the evaporation characteristics obtained in the present MD study with the macroscopic classical thermodynamics in terms of the boiling heat flux using (4) where h_{fg} is the latent heat of evaporation of Ar at the corresponding time averaged temperature (T_{avg}) of the Ar. The values of the time averaged heat flux with the values predicted by classical thermodynamics are tabulated for comparison in Table 3

$$q_{Therm} = h_{fg} \times \dot{m}_{avg} \tag{4}$$

Table 3 provides both atomistic and macroscopic viewpoints of this Letter. The value of the time averaged wall heat flux (q_{avg}) and the thermodynamic prediction of heat flux obtained in the present studies are in well agreement. Table 3 also gives us a proper view point of the extent of the effect of surface materials and wettability on heat transfer. The magnitude of heat fluxes for hydrophilic surfaces is almost three times more than those of hydrophobic surfaces.

4. Conclusion: The evaporation characteristics for a liquid thin film of Ar over a solid surface were diligently studied for different surface materials (Pt, Ag and Al) with different wetting conditions (hydrophilic and hydrophobic) at a constant 130 K temperature. From this Letter, it is evident that the transport phenomena of Ar molecule intimately dependent on the solid–liquid interaction potentials which results in different wetting conditions. As the solid–liquid interaction potential or surface wettability increases, the heat transfer also increases. Different surface materials also affect the evaporation characteristics of thin film Ar. Among the three materials that have been considered in this Letter, Al was the least effective in conducting heat. Pt and Ag showed almost similar characteristics in both wettability conditions. The formation of the non-evaporating layer has been observed for all three materials in hydrophilic case, while thin film evaporation persists for hydrophobic case within the simulation time period. From heat flux point of view, the transfer of heat in case of hydrophilic surface was much higher (almost three times) than the hydrophobic surfaces for all the materials under consideration. The heat transfer characteristics are also compared with the classical thermodynamics viewpoint and it has been observed that, the thermodynamics relationships predict the heat transfer rate quite accurately, especially for the hydrophobic wetting condition.

5 References

[1] Kimura T., Maruyama S.: 'Molecular dynamics simulation of heterogeneous nucleation of a liquid droplet on a solid surface', *Microscale Thermophys. Eng.*, 2002, **6**, (1), pp. 3–13

[2] Yu J., Wang H.: 'A molecular dynamics investigation on evaporation of thin liquid films', *Int. J. Heat Mass Transf.*, 2012, **55**, pp. 1218–1225

[3] Nagayama G., Tsuruta T., Cheng P.: 'Molecular dynamics simulation of bubble formation in a nanochannel', *Int. J. Heat Mass Transfer*, 2006, **49**, (23–24), pp. 4437–4443

[4] Maroo S.C., Chung J.N.: 'Molecular dynamic simulation of platinum heater and associated nanoscale liquid argon (Ar) film evaporation and colloidal adsorption characteristics', *J. Colloid Interface Sci.*, 2008, **328**, pp. 134–146

[5] Morshed A.K.M.M., Paul T.C., Khan J.A.: 'Effect of nanostructures on evaporation and explosive boiling of thin liquid films: a molecular dynamics study', *Appl. Phys. A*, 2011, **105**, pp. 445–451

[6] Hasan M.N., Monde M., Mitsutake Y.: 'Model for boiling explosion during rapid liquid heating', *Int. J. Heat Mass Transf.*, 2011, **54**, (13–14), pp. 2844–2853

[7] Maruyama S., Kimura T.: 'A molecular dynamics simulation of a bubble nucleation on solid surface', *Trans. Jpn. Soc. Mech. Eng. B*, 1999, **65**, (638), pp. 3461–3467

[8] Hens A., Agarwal R., Biswas G.: 'Nanoscale study of boiling and evaporation in a liquid Ar film on a Pt heater using molecular dynamics simulation', *Int. J. Heat Mass Transf.*, 2014, **71**, pp. 303–312

[9] Seyf H.R., Zhang Y.: 'Effect of nanotextured array of conical features on explosive boiling over a flat substrate: a nonequilibrium molecular dynamics study', *Int. J. Heat Mass Transf.*, 2013, **66**, pp. 613–624

[10] Wang W., Zhang H, Tian C., *ET AL.*: 'Numerical experiments on evaporation and explosive boiling of ultra-thin liquid argon film on aluminum nanostructure substrate', *Nanoscale Res. Lett.*, 2015, **10**, p. 158

[11] Zhang H., Li C., Zhao M., *ET AL.*: 'Influence of interface wettability on explosive boiling of ultra-thin liquid films on a heated substrate using molecular dynamics simulation'. Proc. of the 12th IEEE Int. Conf. Nano/Micro Engineered and Molecular Systems, LA, USA, 2017

[12] Zhang H., Li C., Zhao M., *ET AL.*: 'Influence of interface wettability on normal and explosive boiling of ultra-thin liquid films on a heated substrate in nanoscale: a molecular dynamics study', *Micro Nano Lett.*, 2017, **12**, pp. 843–848

[13] Lennard-Jones J.E., Devonshire A.F.: 'Critical phenomena in gases – I', *Philos. Proc. R. Soc. Lond. A, Math. Phys. Sci.*, 1937, **163**, (912), pp. 53–70

[14] 'LAMMPS user's manual' (Sandia National Laboratories, USA), http://lammps.sandia.gov

[15] Humphrey W., Dalke A., Schulten K.: 'VMD: visual molecular dynamics', *J. Comput. Phys.*, 1996, **117**, (1), pp. 1–19

[16] Gambill W.R., Lienhard J.H.: 'An upper bound for the critical boiling heat flux', *ASME, J. Heat Transf.*, 1989, **111**, (3), pp. 53–70

[17] Nagayama G., Kawagoe M., Tokunaga A., *ET AL.*: 'On the evaporation rate of ultra-thin liquid film at the nanostructured surface: a molecular dynamics study', *Int. J. Thermal Sci.*, 2010, **49**, pp. 59–66

doi: 10.1049/mnl.2017.0198